JOURNAL OF Materials CHEMISTRY

Divalent magnesium ion conducting characteristics in phosphate based solid electrolyte composites

Nobuhito Imanaka, Yusuke Okazaki and Gin-ya Adachi*

Department of Applied Chemistry, Faculty of Engineering, Osaka University, 2-1 Yamadaoka, Suita, Osaka, 565-0871, Japan. E-mail: adachi@chem.eng.osaka-u.ac.jp

Received 6th December 1999, Accepted 8th March 2000
Published on the Web 12th April 2000

The divalent Mg^{2+} ion conducting solid electrolyte was synthesized with a composite form by intentionally changing the starting material mixing ratio to the nonstoichiometric region. By such a preparation technique, spontaneous and microscopic dispersion of the secondary $Zr_2O(PO_4)_2$ phase was successfully realized and the Mg^{2+} ion conductivity was considerably enhanced by dispersing the secondary phase, showing the highest conductivity among the Mg^{2+} ionic conducting solid electrolytes reported. The Mg^{2+} migration in the composite solid was clearly demonstrated by dc electrolysis and the Mg^{2+} ion transference number was precisely determined to be unity by a modified Tubandt method. The development of pure Mg^{2+} ion conducting phosphate based solid electrolytes with high stability and considerably high ionic conductivity contributes greatly to opening a new door for the application of advanced materials such as rechargeable batteries and other specific sensor elements.

Introduction

Solid electrolytes in which specific ionic species migrate in solids have already been put on the market. Representative ionic species include monovalent ions such as alkali metal ions, and halide ions, used for batteries[1] and ion sensors.[2] Another representative is the oxide ion (O^{2-}); oxide ion conductors have been commercialized since 1976 as the main component of the oxygen sensor tip.

In contrast, solid electrolytes with divalent cation species such as Mg^{2+},[3–7] alkaline earth cations such as Ca^{2+},[8–11] Sr^{2+},[10–12] Ba^{2+},[10–12] and transition metal ions like Cd^{2+},[10,12] Zn^{2+},[10] Mn^{2+},[10] with the β″-alumina type structure, have been prepared. However, their ionic conductivity is still too low to be utilized in a commercial application. For the purpose of realizing a suitable divalent ion conducting solid electrolyte, the mobile ionic species should be selected from the viewpoint of its ionic radius and stability. Among divalent cations, magnesium ion has the advantage of a stable oxidation state (+2) and a small ionic size. In addition, magnesium metal is one of the suitable candidates for an electrode material in rechargeable batteries with Mg^{2+} ion conducting solid electrolytes because magnesium metal is less reactive than elements of the alkali metal series. In order to realize a practical application, the solid electrolyte itself should be stable in various atmospheres and the counter anion should be selected from a stability point of view, which favors the use of adequate oxides. In order to realize reasonably high divalent Mg^{2+} ion conduction in solids, the solid should contain higher valent cation species in comparison to the mobile Mg^{2+} ion, which bonds strongly to oxide anions to prevent the oxide ion conduction and makes such surroundings for the magnesium ions migrate more smoothly. By considering the above mentioned issues, the most suitable solids we selected are phosphate based materials in which pentavalent P^{5+} exists in addition to tetravalent Zr^{4+} and also contains divalent migrating Mg^{2+} ion. In our previous communication,[13] the enhancement of the divalent ion conductivity was realized by simultaneously dispersing the secondary $Zr_2O(PO_4)_2$ phase during the preparation procedure to form a composite.

In this paper, the Mg^{2+} ion conducting solid composites were successfully synthesized by simultaneously dispersing the secondary phase during the preparation process and the Mg^{2+} ion conducting characteristics were quantitatively investigated in detail.

Experimental

Sample preparation

$MgHPO_4{\cdot}3H_2O$ (purity: 99%), $ZrO(NO_3)_2{\cdot}2H_2O$ (purity: 99%), and $NH_4H_2PO_4$ (purity: 99%) were mixed in a molar ratio of $(1+x):(4+2x):(5+x)$ and heated at 300 °C for 5 h and then 1200 °C for 12 h in air. Since the stoichiometric ratio is 1:4:5 for the $MgZr_4P_6O_{24}$ single phase preparation, zirconium oxide phosphate forms and is microscopically dispersed as a secondary phase. The composite powder was pressed into pellets and sintered at 1200 °C for 12 h in air.

Measurements

The sample characterization was performed by X-ray powder diffraction (XRD) using Cu-Kα radiation (M18XHF, Mac Science). The XRD data were collected by a step-scanning method for the 2θ range from 10° to 120° with a step width of 0.02° and a scan time of 4 s. The electrical conductivity measurements were performed for the sintered pellet with the Pt electrode attached to both surfaces with Pt paste (TR-7601) from Tanaka Kikinzoku Kogyo K. K. by a complex impedance method in the frequency range between 5 Hz and 13 MHz (Precision LCR meter 4192A, Hewlett Packard) in the temperature range from 200 to 800 °C. The polarization behavior was measured by applying a constant current of 0.1 μA between the two Pt electrodes and the voltage generated was monitored as a function of time. The dc conductivity was calculated from the voltage, the applied current, the surface area and the thickness of the pellet sample. For the purpose of directly and quantitatively identifying the mobile charge carrier in the composite, dc electrolysis and the modified Tubandt method[14] were carried out with two platinum plates as the electrodes by applying a voltage of 4 V for 360 h at 800 °C and 6 V for 816 h at 800 °C in air, respectively. After the electrolysis, the cathodic surface of the composite was analyzed by scanning electron microscopy (SEM, S-800, Hitachi), and

electron probe microanalysis (EPMA-1500, Shimadzu). The electrolyzed samples were mounted in a epoxy resin, then cut before cross-sectional EPMA line analysis was carried out in the direction from anode to cathode. The Archimedes method was applied for the relative density calculation and the density of the pellet was calculated by dividing the sintered pellet density by the powder density.

Results and discussion

The X-ray powder diffraction (XRD) patterns of $MgZr_4P_6O_{24}$, $Zr_2O(PO_4)_2$, and the $Mg_{1+x}Zr_4P_6O_{24+x}+xZr_2O(PO_4)_2$ composites with $x=0.2$, 0.4 and 0.5 are shown in Fig. 1. From the XRD analyses, all composites were identified to be a two phase mixture of $MgZr_4P_6O_{24}$ and $Zr_2O(PO_4)_2$. By intentionally increasing the mixing ratio of x from $1:4:5$ to $(1+x):(4+2x):(5+x)$, the intensities of the secondary $Zr_2O(PO_4)_2$ phase toward the $MgZr_4P_6O_{24}$ phase increased monotonously. The lattice parameters a, b, and c are constant at 0.883, 0.892, and 1.243 nm, respectively, for all the systems presented in Fig. 1, similar to the case for $Mg_{1.15}Zr_4P_{5.7}Si_{0.3}O_{24}$,[7] which is reported to also be a two phase mixture of the mother $MgZr_4P_6O_{24}$ phase and the $Zr_2O(PO_4)_2$ phase.

Fig. 2 presents the variation of the logarithm of the conductivity at 800 °C with the $Zr_2O(PO_4)_2$ content in the $Mg_{1+x}Zr_4P_6O_{24+x}+xZr_2O(PO_4)_2$ composite. Here, the composites obtained are expressed as $Mg_{1+x}Zr_4P_6O_{24+x}+xZr_2O(PO_4)_2$, because the composites are composed of only two phases of $MgZr_4P_6O_{24}$ and $Zr_2O(PO_4)_2$ and the mixing ratio of the above mentioned starting materials is $(1+x):(4+2x):(5+x)$ as described above. Upon increasing the $Zr_2O(PO_4)_2$ amount in the composite, the conductivity is

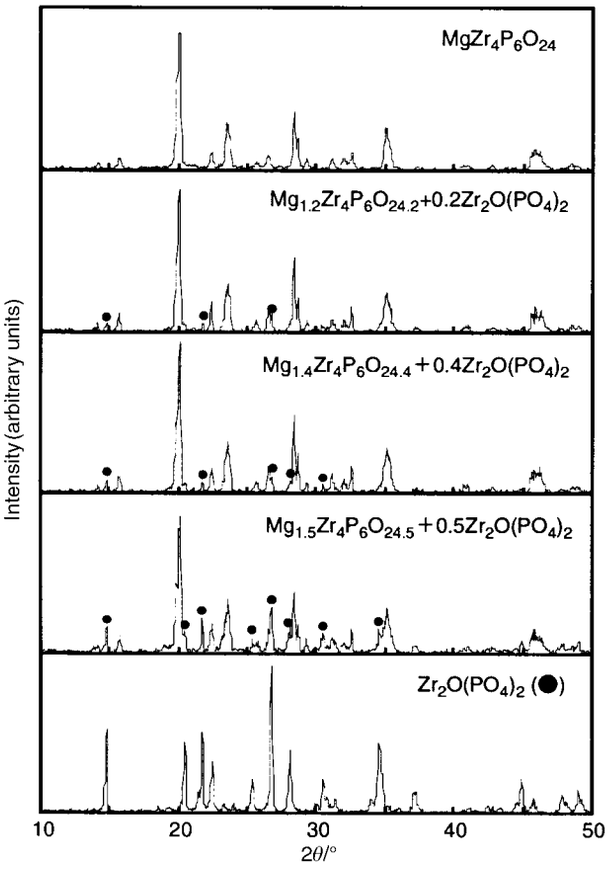

Fig. 1 The X-ray powder diffraction (XRD) patterns of $MgZr_4P_6O_{24}$, $Zr_2O(PO_4)_2$, and the $Mg_{1+x}Zr_4P_6O_{24+x}+xZr_2O(PO_4)_2$ composites with $x=0.2$, 0.4 and 0.5.

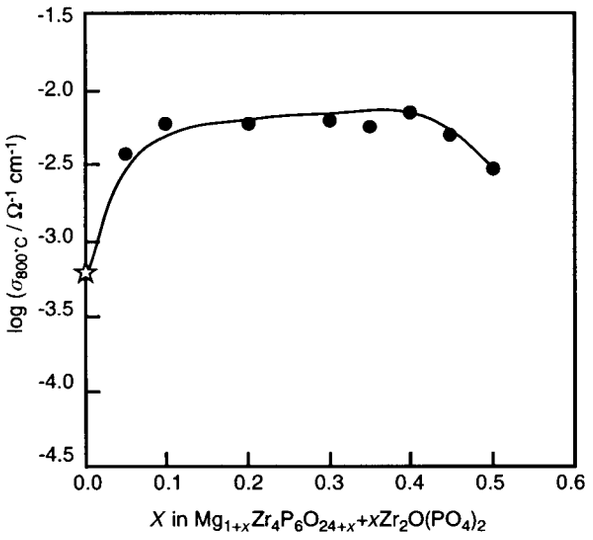

Fig. 2 The variation of the logarithm of the conductivity at 800 °C with the $Zr_2O(PO_4)_2$ content in the $Mg_{1+x}Zr_4P_6O_{24+x}+xZr_2O(PO_4)_2$ composite. ☆ is the datum for pure $MgZr_4P_6O_{24}$.

monotonously enhanced and a maximum value of $6.92\times10^{-3}\ \Omega^{-1}\ cm^{-1}$ was obtained at 800 °C for the composite with $x=0.4$ in $Mg_{1+x}Zr_4P_6O_{24+x}+xZr_2O(PO_4)_2$. The relative densities of $MgZr_4P_6O_{24}$ and the composites with $x=0.4$ and 0.5 were measured and were identified to be 93.1, 99.3, 94.6%, respectively, while the relative density of $Mg_{1.15}Zr_4P_{5.7}Si_{0.3}O_{24}$[5] is reported to be *ca.* 92%. The considerable increase in the electrical conductivity is mainly ascribed to the increase in the density. For the composites with x higher than 0.4, the conductivity reduces because of both the density decrease and the increase of insulating $Zr_2O(PO_4)_2$ volume in the composite. By dispersing the secondary $Zr_2O(PO_4)_2$ phase simultaneously during the preparation procedure, the conductivity of the composite with $x=0.4$ increases by almost one order of magnitude in comparison to that of pure $MgZr_4P_6O_{24}$ without any $Zr_2O(PO_4)_2$ dispersion.

Fig. 3 shows the temperature dependence of the electrical conductivity for the $Mg_{1+x}Zr_4P_6O_{24+x}+xZrO(PO_4)_2$ ($x=0.4$) composite, which shows the highest conductivity in the composite series. The electrical conductivity variations for other Mg^{2+} ion conductors such as $MgZr_4P_6O_{24}$[7] and $Mg_{1.15}Zr_4P_{5.7}Si_{0.3}O_{24}$[7] are also depicted. The electrical conductivity of the present composite is one order of magnitude higher compared to that of pure $MgZr_4P_6O_{24}$, in the whole temperature range examined.[7] Even in comparison to $Mg_{1.15}Zr_4P_{5.7}Si_{0.3}O_{24}$,[7] which has been reported to exhibit the highest Mg^{2+} ion conductivity, the conductivity of the present composite is still 2.3 times higher. The conductivity of the secondary $Zr_2O(PO_4)_2$ phase is also measured and shown in Fig. 3. The conductivity of the oxide phosphate is more than two orders of magnitude lower than that of the composite and this result explicitly demonstrates that the $Zr_2O(PO_4)_2$ phase exists as insulating secondary particles in the composite. The formation of the insulating $Zr_2O(PO_4)_2$ secondary phase in the composite contributes greatly to increasing the conductivity of the composite and the highest effects were observed for the $Mg_{1+x}Zr_4P_6O_{24+x}+xZr_2O(PO_4)_2$ ($x=0.4$) composite. The activation energies were found to be 135.8 kJ mol^{-1} and 141.5 kJ mol^{-1} for $Mg_{1+x}Zr_4P_6O_{24+x}+xZr_2O(PO_4)_2$ ($x=0.4$) and pure $MgZr_4P_6O_{24}$, respectively. The higher sinterability of the composite results in an enhancement of the relative density and reduces the activation energy to improve the electrical conducting characteristics in the grain boundaries.

Fig. 4 presents the oxygen partial pressure dependence of the electrical conductivity at 700 °C. The electrical conductivity

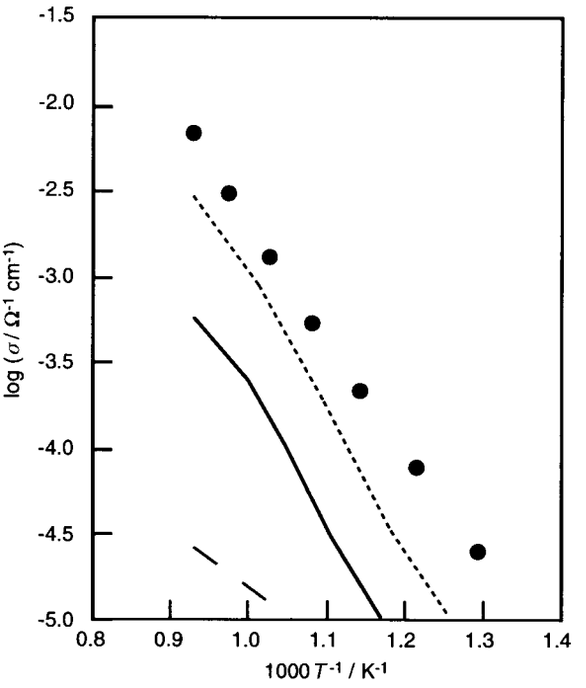

Fig. 3 The temperature dependence of the electrical conductivity for the composite of $Mg_{1+x}Zr_4P_6O_{24+x}+xZr_2O(PO_4)_2$ ($x=0.4$) (●), which shows the highest conductivity in the composite series. Solid, dotted, and dashed lines are the data reported for $MgZr_4P_6O_{24}$,[7] $Mg_{1.15}Zr_4P_{5.7}Si_{0.3}O_{24}$,[7] and $Zr_2O(PO_4)_2$, respectively.

was constant in the wide oxygen partial pressure region from 10^{-17} Pa to 10^5 Pa, indicating no hole or electron type semiconducting behavior appears and also demonstrating a considerably high stability in such a wide oxygen pressure region.

The time dependence of the σ_{dc}/σ_{ac} ratio was monitored and is depicted in Fig. 5. Here, σ_{dc} and σ_{ac} represent the conductivity obtained by dc and by ac measurements, respectively. An abrupt decrease from 1.0 to below 0.02 in the ratio was similarly recognized in both oxygen (P_{O_2}: 10^5 Pa) and helium (P_{O_2}: 4 Pa) atmosphere as shown in the insert. The same high polarization behavior clearly excludes the probability of oxide ion (O^{2-}) conduction in the composite as reported in our previous paper.[15] In addition, the considerable polarizing phenomenon indicates that neither electrons nor holes are the mobile species in the composite. Furthermore, the polarization measurements were also carried out in dry and wet (H_2O: 0.6 vol%) air atmospheres as plotted in Fig. 6. While a slight decrease was observed in the wet atmosphere, the polarization was as high as below 0.02 after 2 s and a considerably high polarizing

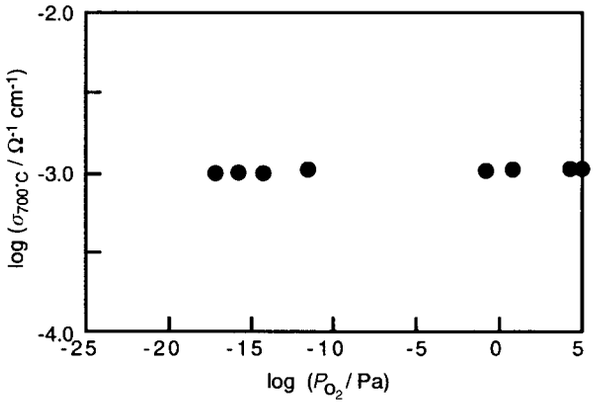

Fig. 4 The oxygen partial pressure dependence of the electrical conductivity for $Mg_{1+x}Zr_4P_6O_{24+x}+xZr_2O(PO_4)_2$ ($x=0.4$) at 700 °C.

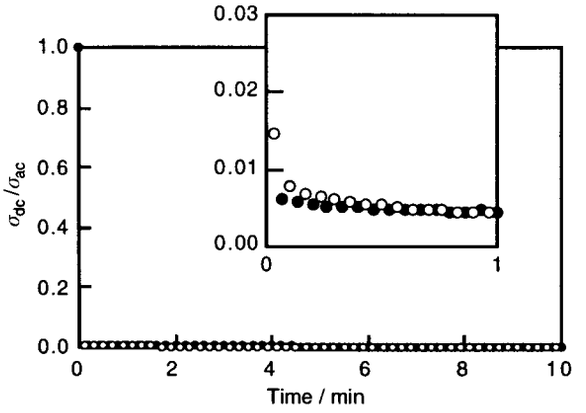

Fig. 5 The time dependences of the σ_{dc}/σ_{ac} ratio in both oxygen (●) (P_{O_2}: 10^5 Pa) and helium (○) (P_{O_2}: 4 Pa) atmosphere for the $Mg_{1+x}Zr_4P_6O_{24+x}+xZr_2O(PO_4)_2$ ($x=0.4$) composite at 700 °C. σ_{dc} and σ_{ac} represent the conductivity obtained by dc and by ac measurements, respectively. Inset shows the magnified view in the early stages.

phenomenon was similarly observed. From this phenomenon, proton (H^+) conduction in the composite is also disproved. Therefore, the migrating species are limited to only cationic species, that is, Mg^{2+}, Zr^{4+}, P^{5+}.

For the purpose of identifying the mobile cation species in the $Mg_{1+x}Zr_4P_6O_{24+x}+xZr_2O(PO_4)_2$ ($x=0.4$) composite, direct dc electrolysis (4 V for 360 h at 800 °C) of the composite sample was performed with two platinum electrodes (the decomposition voltage of the composite had already been estimated to be *ca.* 3 V from the *I–V* relationship). By the observation of the composite surface which had been in contact with the Pt cathodic electrode during the electrolysis by SEM, a number of round cluster deposits were recognized as shown in Fig. 7. From EPMA spot analysis, the elements within these deposits were identified as Mg, P, Zr and the ratios of Mg/(P+Zr) and P/Zr are 1.44 and 3.36, respectively (Fig. 8(a)). In the bulk composite before the electrolysis, the observed ratios of Mg/(P+Zr) and P/Zr were 0.12 and 1.41, respectively (Fig. 8(b)). Despite the fact that some deviation of the peak ratio is commonly observed in the case of spot analysis of composite materials, a considerable amount of Mg segregation, that is, 12.4 times higher in the Mg/(P+Zr) ratio is recognized, while the increase of the P/Zr peak ratio is only 2.38 times on the cathodic surface. These phenomena explicitly mean that the predominant segregating species is magnesium.

In addition, for the purpose of directly and quantitatively identifying the mobile species in the $Mg_{1+x}Zr_4P_6O_{24+x}+xZr_2O$

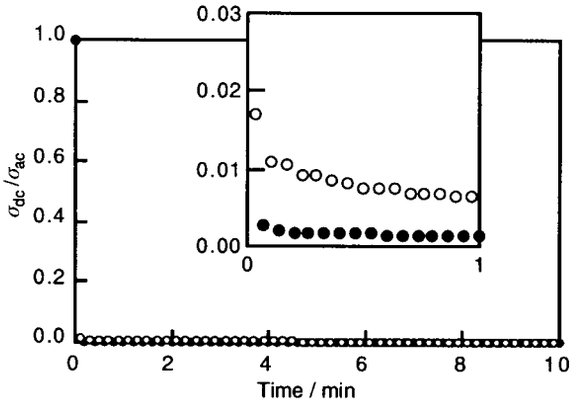

Fig. 6 The time dependences of the σ_{dc}/σ_{ac} ratio in dry air (●) and wet air (H_2O: 0.6 vol%) (○) for the $Mg_{1+x}Zr_4P_6O_{24+x}+xZr_2O(PO_4)_2$ ($x=0.4$) composite at 800 °C. Inset shows the magnified view in the early stages.

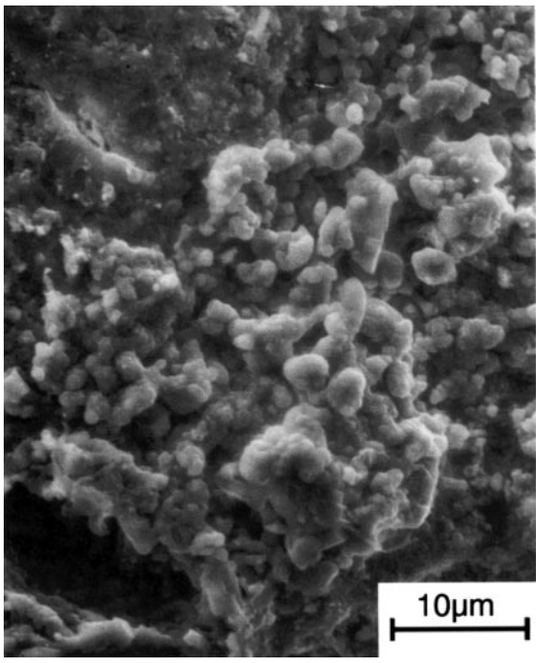

Fig. 7 SEM photograph of the cathodic surface of $Mg_{1+x}Zr_4P_6O_{24+x}+xZr_2O(PO_4)_2$ ($x=0.4$) after electrolysis.

$(PO_4)_2$ ($x=0.4$) composite, the modified Tubandt electrolysis method was carried out as illustrated in Fig. 9. The change of the weight after the electrolysis was measured for the anodic part (A + Pt(Anode)), the middle composite electrolyte (B), and the cathodic part (C + Pt(Cathode)) and the results are listed in

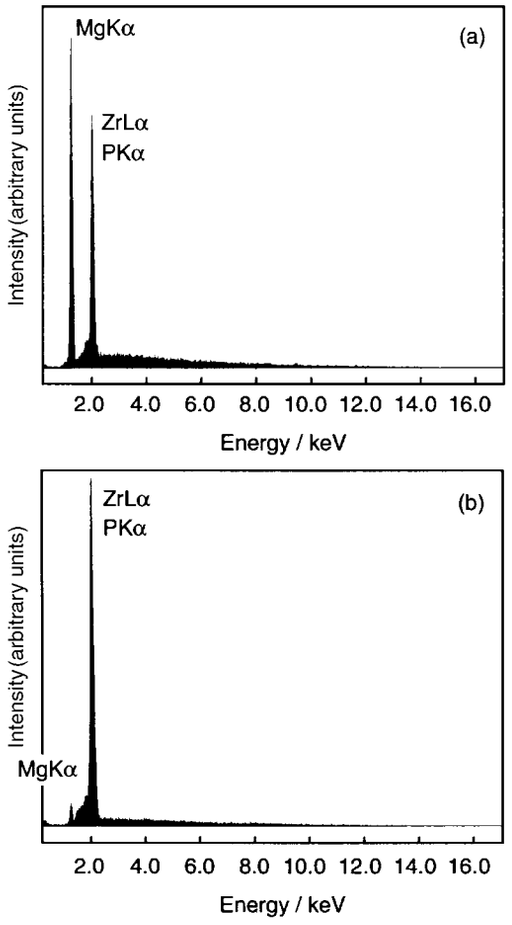

Fig. 8 EPMA spot analysis results of the deposits on the cathodic surface (a) and that of the bulk $Mg_{1+x}Zr_4P_6O_{24+x}+xZr_2O(PO_4)_2$ ($x=0.4$) composite (b).

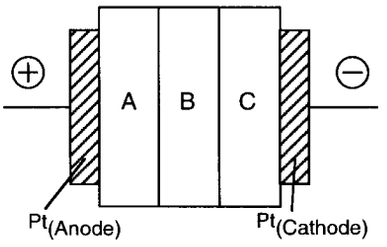

Fig. 9 The setup of the modified Tubandt electrolysis.

Table 1 The changes in weight after the electrolysis: 6 V at 800 °C for 816 h

		Change in weight of tablet/mg			
Tablet	Observed value	Mg^{2+}	Zr^{4+}	P^{5+}	O^{2-}
C + Pt(Cathode)	1.00	0.99	1.51	0.70	0
B	0.06	0	0	0	0
A + Pt(Anode)	−1.10	−0.99	−1.51	−0.70	0

Table 1. Since the weight increase and decrease were observed in the cathodic and anodic parts, the mobile ion is identified as a cation species, as elucidated from the results described above. The expected weight change for the cations of Mg^{2+}, Zr^{4+} and P^{5+} can be calculated from the total charge of 4.7 C as reported in the table. From the table, the mobile ion species is definitely identified as Mg^{2+} ion and the Mg^{2+} ion transference number is estimated to be unity from the weight change.

Fig. 10 depicts the results of the EPMA line analyses of the three pellets used for the modified Tubandt electrolysis. Considerably high segregation was clearly observed for the composite pellet (C) of the cathodic side area. In contrast, both Zr and P intensities decreased on the same area where the high Mg segregation was observed because the detected element is predominantly Mg in this area.

From the polarization and the modified Tubandt electrolysis results described above, the predominant mobile species in the $Mg_{1+x}Zr_4P_6O_{24+x}+xZr_2O(PO_4)_2$ ($x=0.4$) composite is expli-

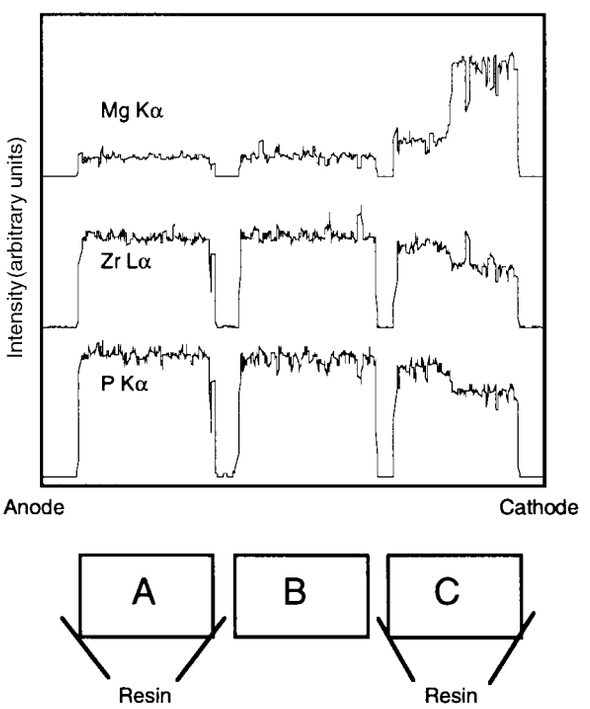

Fig. 10 The results of the modified EPMA line analyses of the three pellets used for the Tubandt electrolysis.

citly identified to be the divalent magnesium (Mg^{2+}) cation. The divalent Mg^{2+} ion conductivity enhancement is predominantly attributed to the considerable enhancement in its relative density due to the microscopic dispersion of the $Zr_2O(PO_4)_2$ secondary phase in the composite.

Acknowledgements

The present work was partially supported by a Grant-in-Aid for Scientific Research No. 09215223 on Priority Areas (No. 260), Nos. 06241106, 06241107, and 093065 from The Ministry of Education, Science, Sports and Culture. This work was also supported by the "Research for the Future, Preparation and Application of Newly Designed Solid Electrolytes (JSPS-RFTF96P00102)" Program from the Japan Society for the Promotion of Science.

References

1 T. Kudo and K. Fueki, *Solid State Ionics*, Kodansha and VCH, 1990, p. 177.
2 M. S. Frant and J. W. Ross, Jr., *Science*, 1966, **154**, 1553.
3 S. Ikeda, M. Takahashi, J. Ishikawa and K. Ito, *Solid State Ionics*, 1987, **23**, 125.
4 K. Nomura, S. Ikeda, K. Ito and H. Einaga, *Bull. Chem. Soc. Jpn.*, 1992, **65**, 3221.
5 K. Nomura, S. Ikeda, K. Ito and H. Einaga, *Chem. Lett.*, 1992, 1897.
6 K. Nomura, S. Ikeda, K. Ito and H. Einaga, *Solid State Ionics*, 1993, **61**, 293.
7 K. Nomura, Ph.D. Thesis, Nagoya Institute of Technology, Nagoya, Japan, 1993.
8 G. Dorner, H. Durakpasa, G. Fafilek and M. W. Breiter, *Solid State Ionics*, 1992, **53–56**, 553.
9 K. W. Semkow and A. F. Sammells, *J. Electrochem. Soc.*, 1988, **135**, 244.
10 G. C. Farrington and B. Dunn, *Solid State Ionics*, 1982, **7**, 267.
11 R. Seevers, J. DeNuzzio, G. C. Farrington and B. Dunn, *J. Solid State Chem.*, 1983, **50**, 146.
12 B. Dunn and G. C. Farrington, *Mater. Res. Bull.*, 1980, **15**, 1773.
13 N. Imanaka, Y. Okazaki and G. Adachi, *Chem. Lett.*, 1999, 939.
14 C. Tubandt, *Handb. Exp. Phys.*, 1932, **7**, 1.
15 Y. Kobayashi, T. Egawa, S. Tamura, N. Imanaka and G. Adachi, *Chem. Mater.*, 1997, **9**, 1649.